MIDAS

MANAGING IMPACTS OF DEEP SEA RESOURCE EXPLOITATION

Project acronym:	MIDAS
Grant Agreement:	603418
Deliverable number:	Deliverable 2.3
Deliverable title:	Report on model simulations of far-field dispersion effects under a range of future climate and extreme future scenarios
Work Package:	WP 2
Date of completion:	23 October 2015

MIDAS

MANAGING IMPACTS OF DEEP SEA RESOURCE EXPLOITATION

Report on model simulations of far-field dispersion effects under a range of future climate and extreme future scenarios

Deliverable 2.3

George Nurser

National Oceanography Centre
European Way
Southampton
SO14 3ZH
United Kingdom

23 October 2015

Contents

1. Introduction

We have modelled pollutant dispersal from possible deep mining sites on the central Mid-Atlantic Ridge, such as the Moreto site (37.35° – 37.65°N, 32.19° - 31.60°W), both in present climate conditions and in the projected future climate at the end of the 21st century. We have produced a 'best estimate' for dispersal in present day conditions using particle trajectories derived from flow fields of the global NEMO http://www.nemo-ocean.eu/ model run at 1/12° horizontal resolution forced by present day atmospheric conditions (Marzocchi et al., 2015). We have estimated dispersal in the projected future climate of the 2090s using trajectories from velocity fields of the ROAM simulation (Yool et al., in press; Aksenov et al., in press), a version of the NEMO model forced by the atmospheric fields of a coupled climate projection run by the Hadley Centre. Unfortunately, due to computational constraints, the ROAM model is not fully eddy-resolving, but has a resolution of a ¼°, and is therefore only 'eddy-permitting', with a weaker eddy field, and is likely to underestimate dispersal. In order to separate the effects of differences in resolution from those of different climate conditions, we also show particle dispersion in a ¼° resolution run of the NEMO model forced by current atmospheric conditions (Blaker et al., 2015).

We first briefly describe the trajectory model, and how it is initialised. We then discuss our 'best estimate' of dispersion for the present day in the fully eddy-resolving model. This followed by studying the reduction in dispersion consequent on coarser resolution but forced by present day climate. Finally we consider the dispersion patterns in the projected climate of the 2090s.

2. The ARIANE trajectory model

Particle trajectories are calculated using code based on v2.2.6_08 of the ARIANE package, a Lagrangian off-line numerical tool developed by Bruno Blanke and Nicolas Grima (Laboratoire de Physique des Oceans; http://stockage.univ-brest.fr/grima/Ariane/; Blanke and Raynaud (1997)). This tool assumes that velocities may be linearly interpolated throughout each tracer cell of the model, so that trajectories can be solved piecewise analytically.

For the studies discussed here, particles are seeded in a 200 x 200 horizontal grid spread evenly over the Moreto site (37.35° N–37.65° N, 32.19°–31.60° W) below the 52nd model layer; that is, at depths between 1584 m and the ocean bottom, which ranges from 2000–2300 m in this area. Particles were seeded at 11 vertical depths spaced regularly in each model layer (thicknesses 140–175 m), i e. the sets of 200 x 200 particles were spaced ~14m apart in the vertical. Fig. 1 shows the seeded volume (white) lying in a valley in the mid-Atlantic Ridge, west of the Azores, superimposed upon the bottom topography from the NEMO 1/12° model.

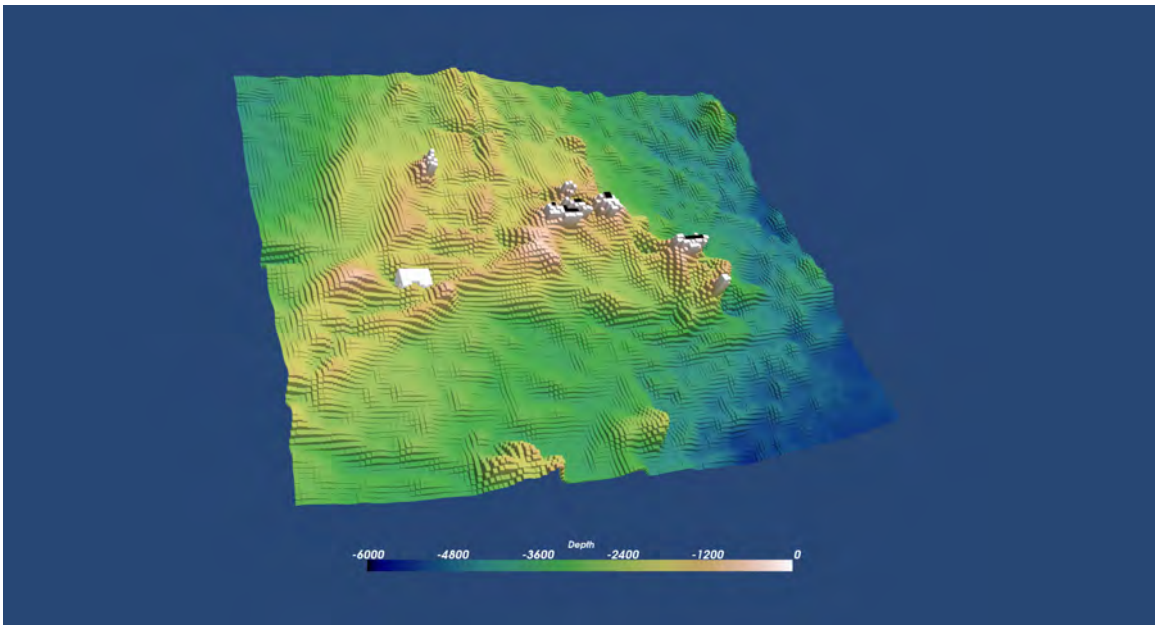

Figure 1: Bottom topography from the 1/12° model around the Azores and the Moreto site (37.35° N–37.65° N, 32.19°–31.60° W), showing (white box) the volume into which the particles are seeded at the start of the runs.

Since the horizontal area under topography increases with depth (and so the sea-area decreases), the cumulative distribution function of particles against height (Fig. 2) grows with height more slowly at greater depths. In total about 1,100,000 particles are seeded in the 1/12° model, but because the 1/4° bottom topography is cruder, there are not so many resolved hollows and ditches in the topography, so parts of the water column are lost, permitting only ~800,000 particles.

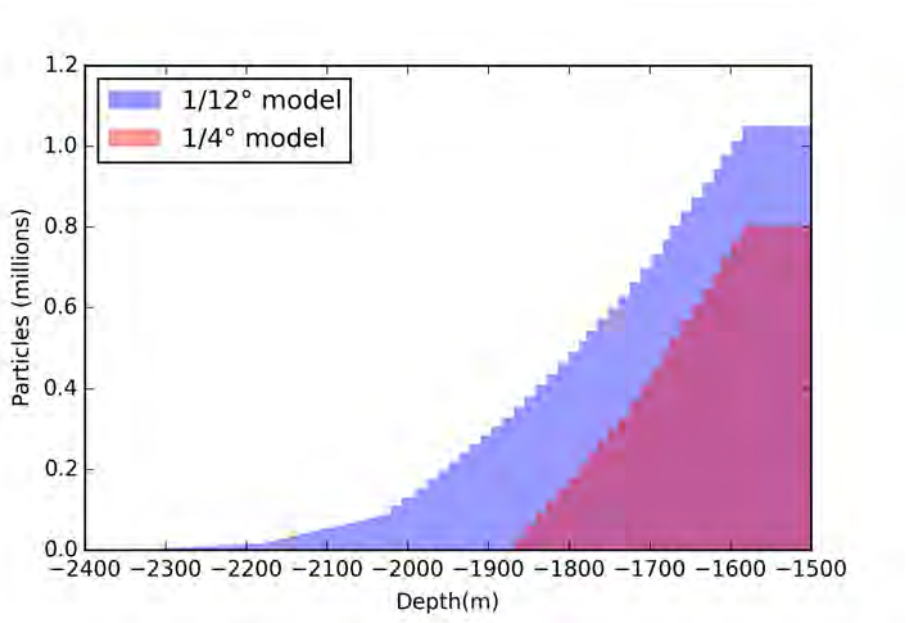

Figure 2: Cumulative distribution function of seeded particles against height for 1.12 ° model (blue) and ¼° (red).

3. Flow in the eddy-resolving model

The flow patterns in the North Atlantic of this eddy-resolving model are fairly reasonable (Marzocchi et al., 2015). The mean kinetic energy (i.e. the squared speed of the mean flow) shows a substantial Gulf Stream recirculation (Fig. 3a) at mid-depths (~1500–2000m), as well as a clear deep western boundary current, while there is considerable eddy kinetic energy (Fig. 3b) even at these relatively quiescent mid-depths. The Montgomery function on a surface of constant steric height passing through the Moreto area at depths of ~1600 m (similar to a surface of constant potential density) is shown in Fig. 3c. This gives streamlines of geostrophic flow on surfaces of constant steric anomaly (McDougall, 1989; Aksenov et al. 2011) analogously to pressure on surfaces of constant geopotential height. A broad anticyclonic circulation is evident over the western North Atlantic but the Moreto area is away from the main flow.

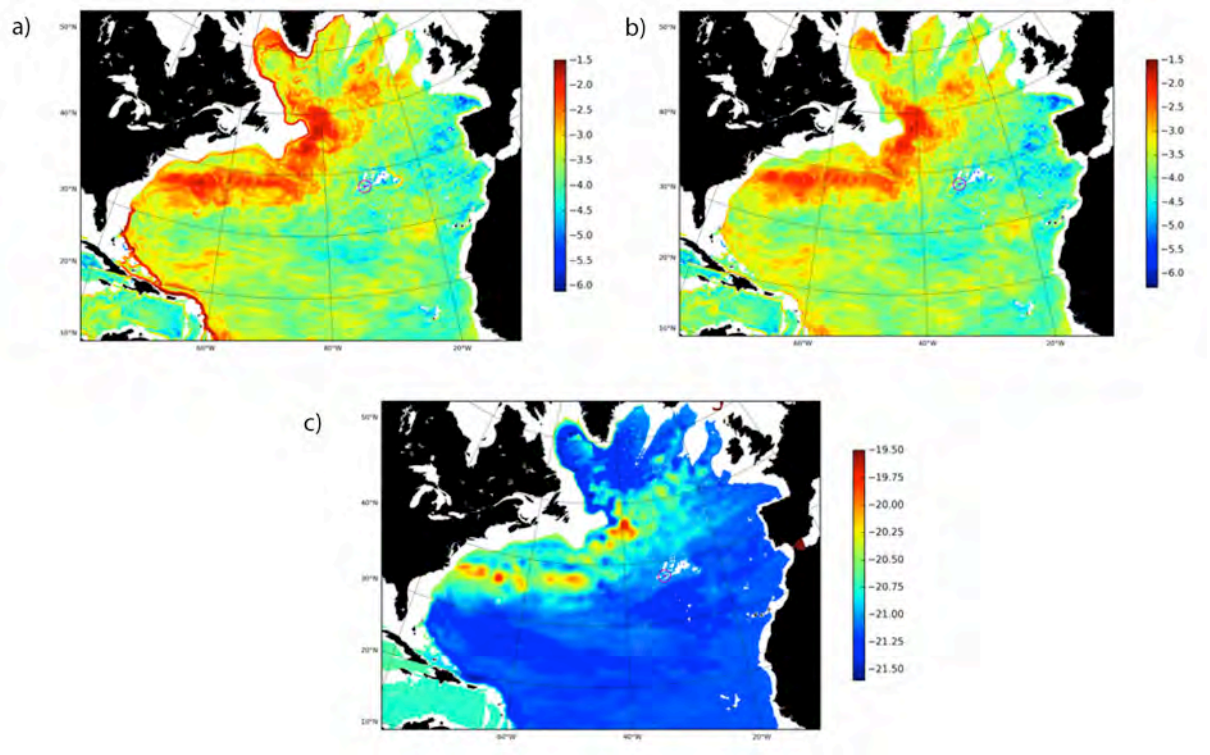

Figure 3: (a, top left): Log10 of the mean kinetic energy in m^2s^{-2}; so a value of –2 corresponds to a speed of ~0.16 m s^{-1}, and –4 to ~0.016 m s^{-1}. (b, top right). Log_{10} of the mean kinetic energy in m^2s^{-2}. (c, bottom). Montgomery function on the 28.6 specific density anomaly surface (σ_2~36.9). The Moreto site is denoted by the rectangle inside the circle.

3.1 Results from the eddy-resolving model

The 1.1 million particles seeded as described above were then tracked by the ARIANE trajectory program over the 10 year period 2001–2010, using 5-day velocity means from the 75 vertical level, eddy-resolving 1/12° horizontal resolution NEMO configuration (Marzocchi et al., 2015). Some (approximately 5%) of the particle positions at 2, 5 and 10 years are shown in 3D in Fig. 4a, b and c.

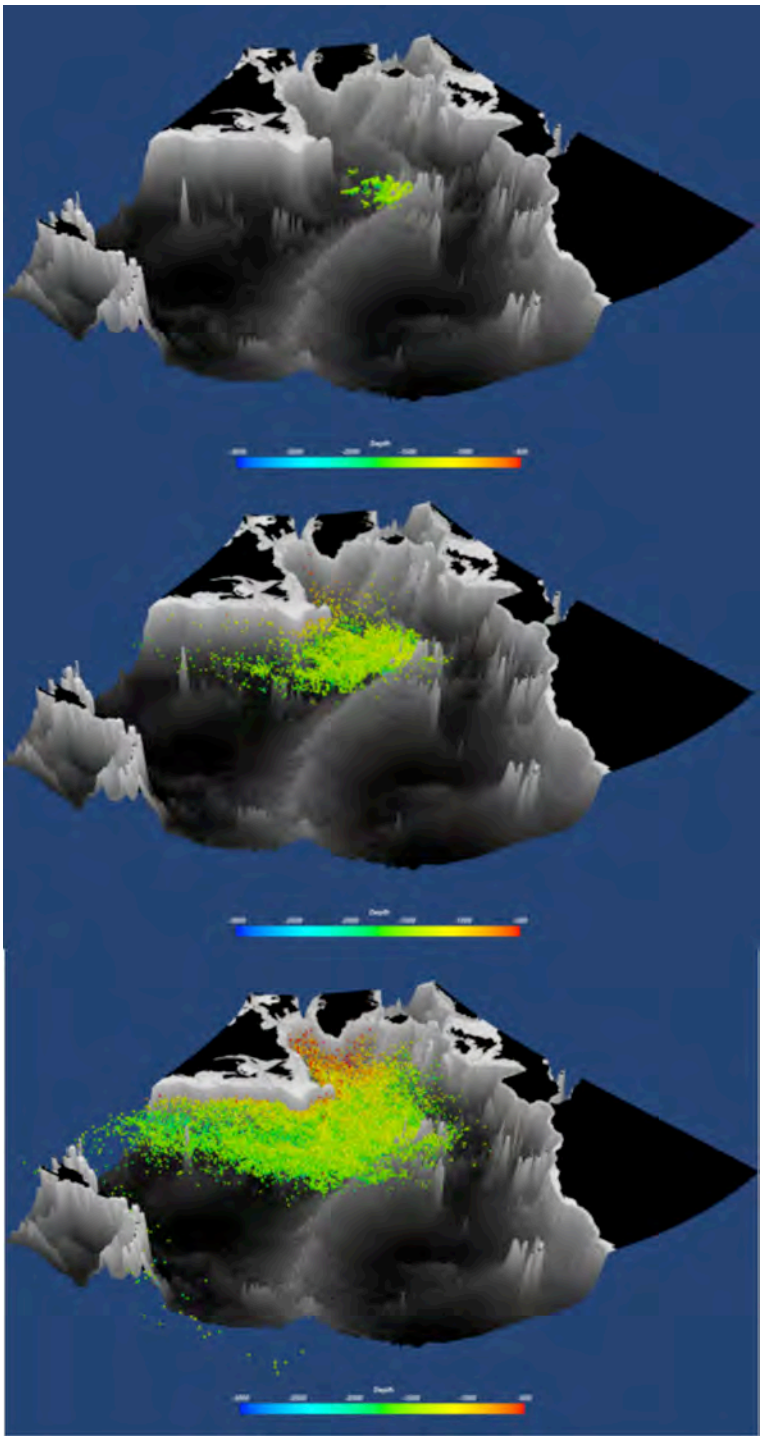

Figure 4: Particle positions at a. (top) 2 yrs, b (middle) 5 yrs and c (bottom) at 10 yrs.

Most particles remain at depths of 1500–1800 m but a few that disperse towards the Labrador Sea move upwards, following the northwards shoaling of the density layers. This vertical spreading and upwards movement is shown more clearly in the histogram Fig. 5a that includes all the particles. The spreading in potential density is more symmetrical (Fig. 5b), as the particles tend to be advected with the density surfaces. However, it may differ from that of a passive tracer advected online by the model as (i) the use of the 5-day means instead of online tracking may cause some spurious movement of particles off density surfaces and (ii) the particles are not subject to the model vertical diffusion.

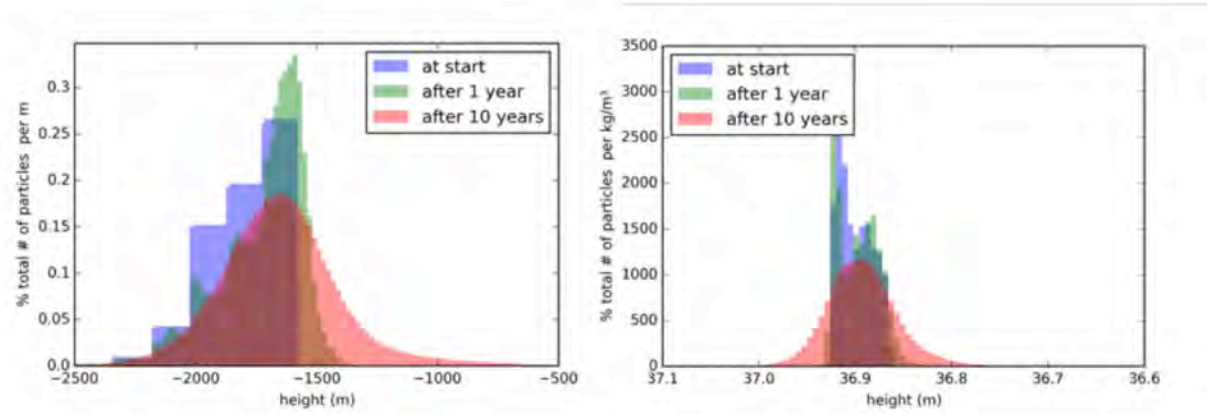

Figure 5a. (left panel): vertical histogram of particle density against depth, given as % of total number of particles per meter. 5b. (right panel) Particle density against potential density referenced to 2000 m. All of the shaded areas integrate to 100%.

Over 10 years, the particles spread mostly westward. Fig. 6a shows the vertically integrated structure of the lateral spreading at this time. Similarly to the plots of vertical dispersion plotted above, the units are % of total number of particles per unit area, where area is in km^2; so the total again integrates out to 100%. There is a tongue of high particle load to the NW of the Moreto site (the blue rectangle in the centre of the blue circle) that continues to the southwest, reaching towards the subtropical gyre at 35°N, 50°W. Fig. 6b shows the total percentage of particles in each horizontal bin 10° in longitude and 10° in latitude. Given that the 10° by 10° bins have areas approximately 10^6 km^2 (at least towards the southern part of the domain) the colorbar scales in Fig. 6a and 6b. are broadly comparable. Note that about a third of the particles remain in the horizontal bin encompassing the seeding point at the Moreto site, and a further quarter lie in the next bin westward. Substantial numbers of particles (>40%) do however escape these two bins, moving further southward and westward, consistent with Fig. 6a. We have investigated the depth variation of the spreading, and find that a larger fraction (60–65%) of the deeper waters tend to remain near the site in these two bins, and a smaller fraction (~45%) of the shallower waters. However the behaviour is not qualitatively different.

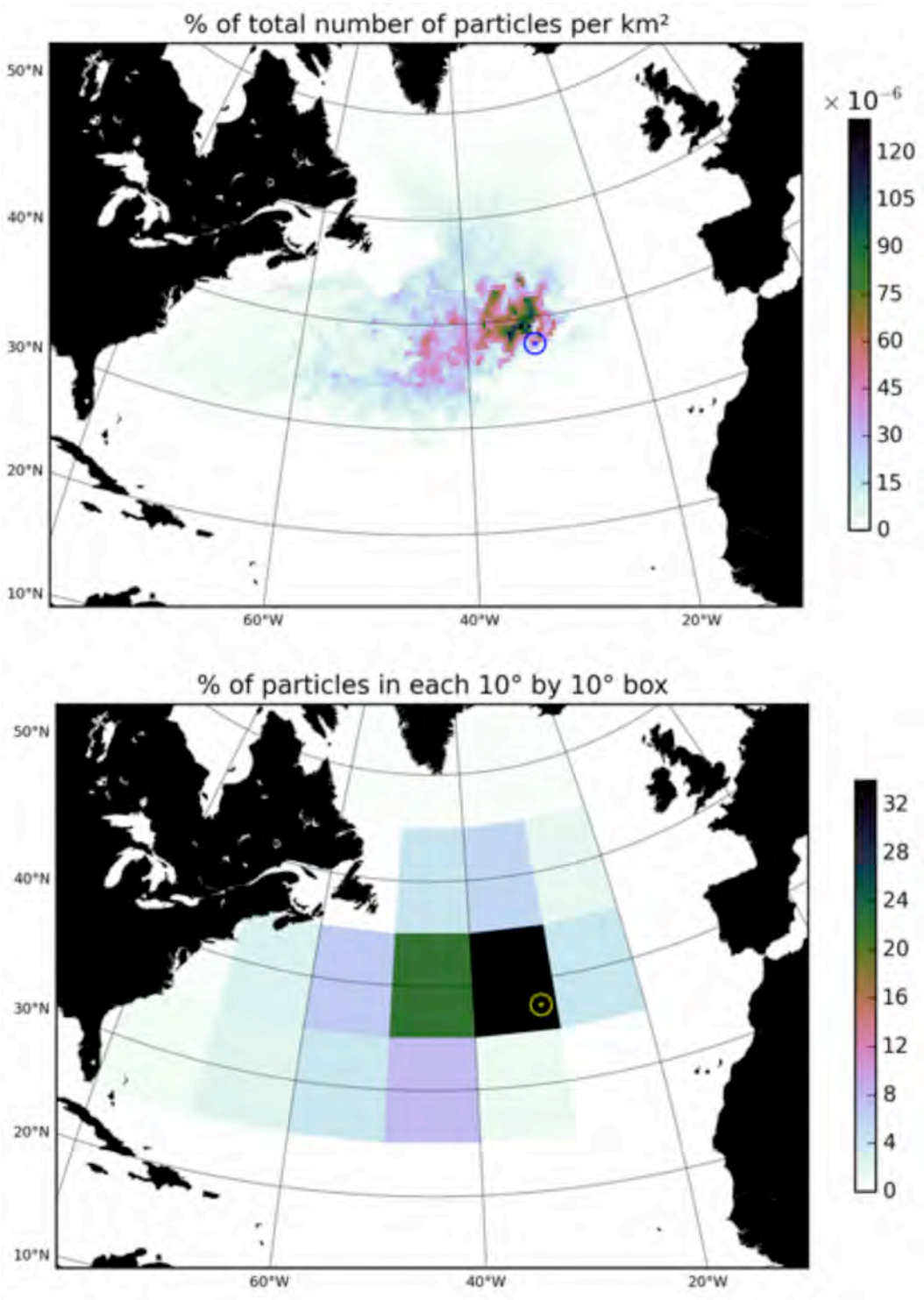

Figure 6a (top panel): Colour-shaded plot of horizontal field of vertically-integrated particle density, given as % of total number of particles per square kilometre. The Moreto site is denoted by the small blue rectangle inside the blue circle. 6b. (bottom panel) % of particles within each of the 10° by 10° bins. Moreto site in yellow.

4. Flow in the 1/4° model with present-day forcing

The surface flow patterns in the North Atlantic of this eddy-permitting model generally lack a vigorous enough eddy field (e.g. Blaker et al., 2015), but are fairly acceptable. The mean kinetic energy (i.e. the squared speed of the mean flow) shows a substantial Gulf Stream recirculation (Fig. 3a) at mid-depths (~1500–2000m), as well as a clear deep western boundary current. In fact the flow speeds appear very similar to those of the eddy resolving 1/12° model (Fig. 3a).

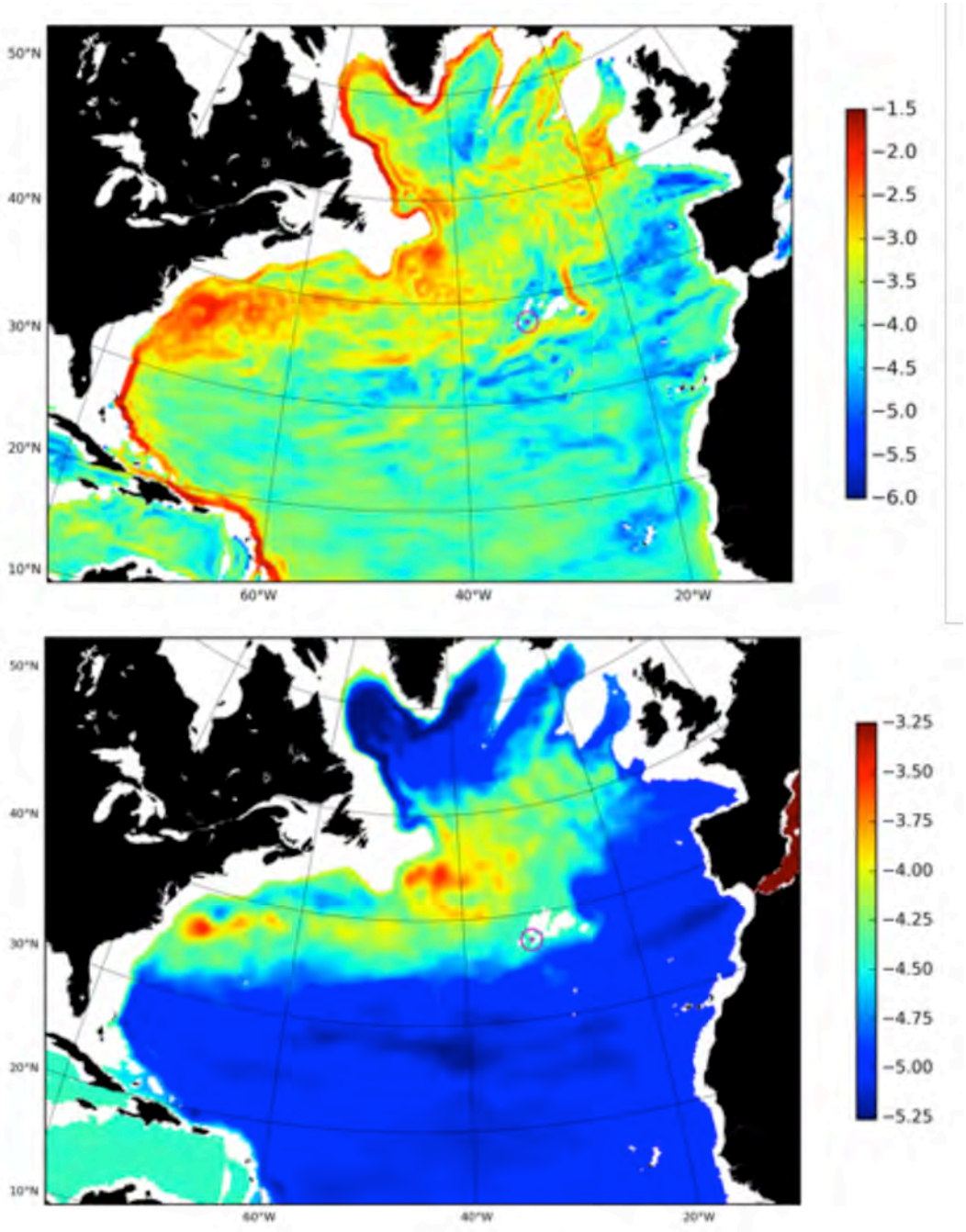

Figure 7 (a, top): Log_{10} of the mean kinetic energy in m^2s^{-2}; (b, bottom). Montgomery function on the specific density anomaly surface approximating σ_2~36.9), as in Fig. 3c.

The Montgomery function is also fairly similar to that in the eddy-resolving model (Fig. 3c); note that although the values are different, the differences and gradients (which drive the flow) are very similar. Note that the Moreto region appears to be in a region of stronger flow here in the eddy-permitting run than it was in the eddy-resolving run.

4.1 Results from the 1/4° model with present-day forcing

The 800,000 particles seeded as described above were then tracked by the ARIANE trajectory program over the 10 year period 1997–2007, using 5-day velocity means from the eddy-resolving 1/4° horizontal resolution NEMO configuration. Again ~5% of the particles are plotted. Note that although dispersion begins more slowly than in the high resolution run, major movement of particles is evident by year 10 after they have moved through the western boundary systems, and e.g. stronger southward movement along the South American coast is evident than in the eddy-resolving run.

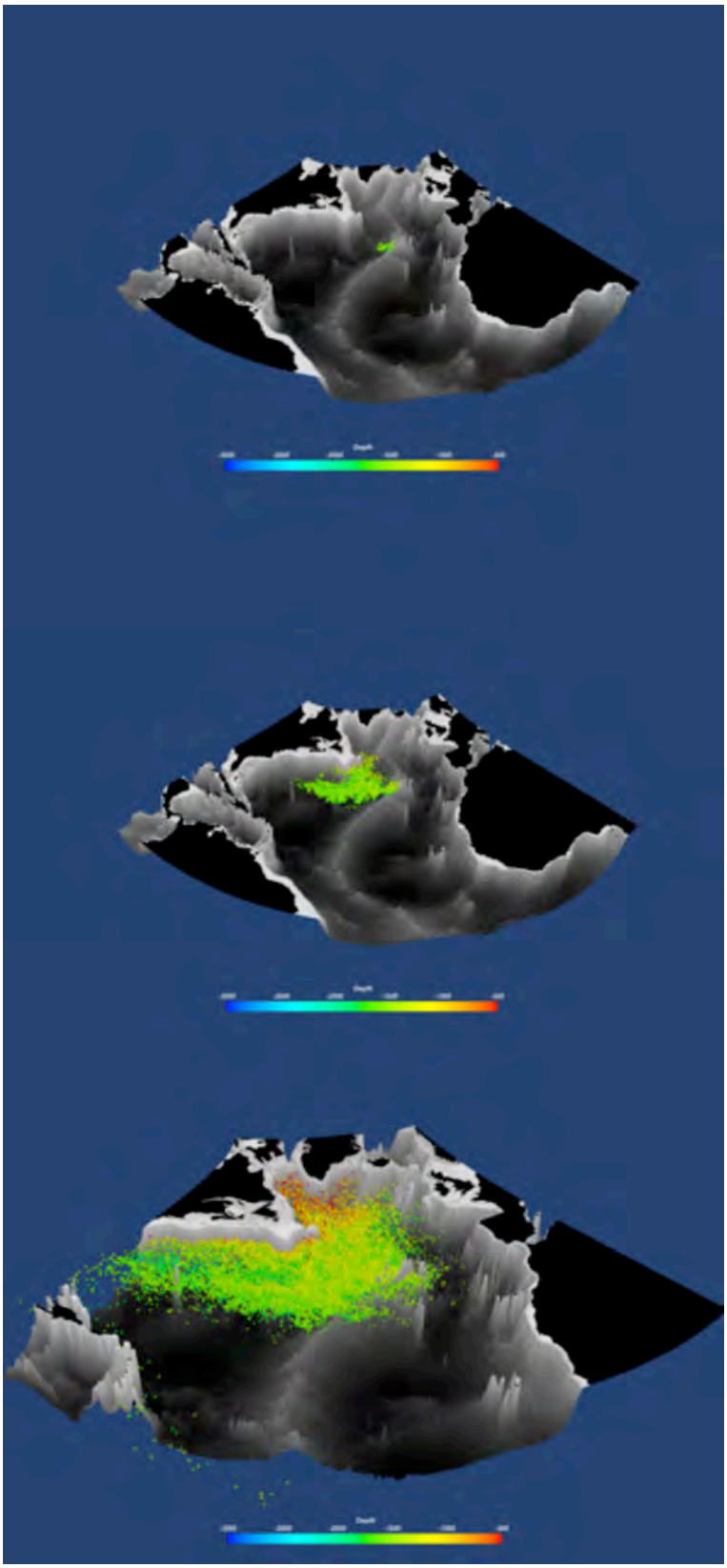

Fig. 9. Particle positions at a. (top) 2 yrs, b (middle) 5 yrs and c (bottom) at 10 yrs for the ¼° model run with forcing from 1997–2007.

Some vertical spreading and upwards movement is evident in the histogram Fig. 10a, though the spreading seems less evident than for the eddy-resolving model (Fig. 5a), partly because the original distribution is more tightly focused (because of the lack of smaller scale topography) but also perhaps because the less turbulent velocities are better temporally resolved by the 5-day means. The spreading in potential density is also less evident, presumably for the same reasons.

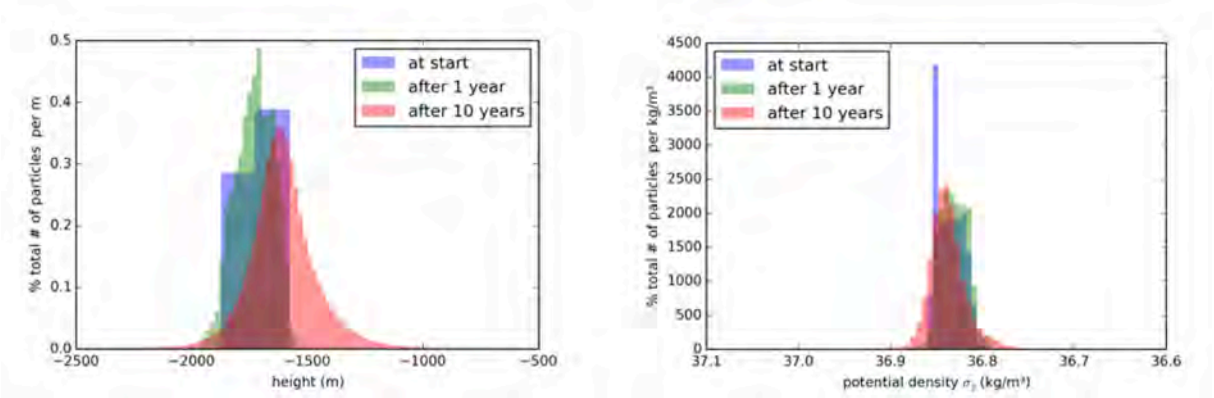

Figure 10a. (left panel): Histogram of particle density against depth, and 10b (right panel) against potential density referenced to 2000 m. As Fig 5, but for the ¼° present-day run.

Lateral spreading over 10 yrs is again mostly westward, but unexpectedly, it is considerably more striking than in the 1/12° model. Fig. 11a (analogous to 6a) shows that the structure of the vertically integrated lateral spreading looks very different to that of the 1/12° model at this time. Apart from a patch of particles immediately to the NW of the Moreto site, the major mass of particles has moved westwards to between 50° and 80° W and along the line of the 30° N parallel. The coarse binning in Fig. 11b emphasizes how different the distribution is; about 30% of the particle load is now between 60° and 50° W, while the bins between 40° and 30° W near the Azores that previously held ~55–60% of the particles now hold only about 10–14%.

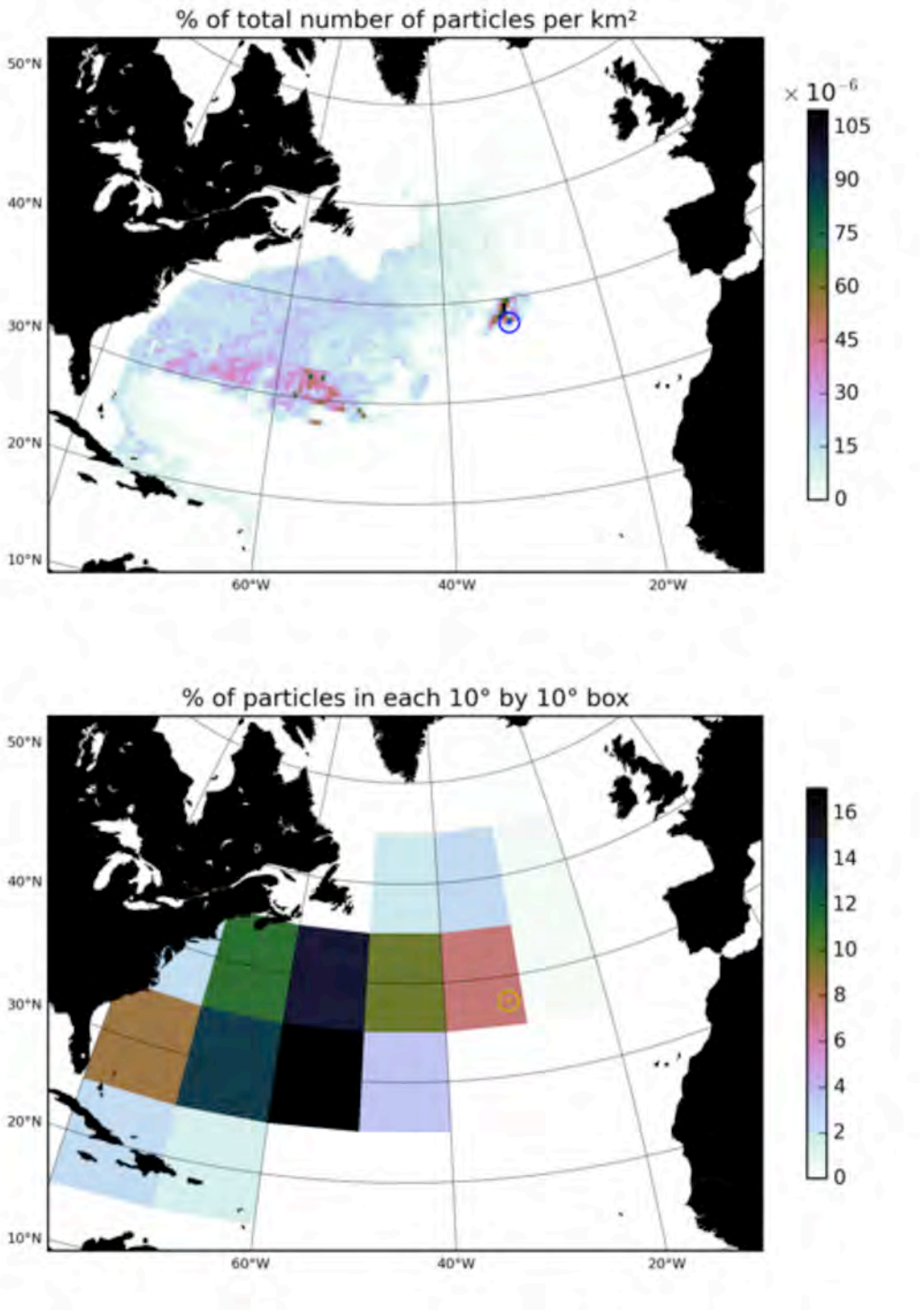

Figure 11a (top panel): Colour-shaded plot of horizontal field of vertically-integrated particle density, given as % of total number of particles per square kilometre. 11b. (bottom panel) % of particles within each of the 10° by 10° bins. Both for the eddy-permitting ¼° model run with present day forcing

5. Flow in the 1/4° model forced by the atmosphere of the 2090s

The Hadley centre of the UK Met Office has made climate projections for the next century. We use those projections here (Yool et al., in press; Aksenov et al.; in press) to provide atmospheric air temperatures, winds, downwelling long wave and solar radiation, as well as precipitation. These projected atmospheric properties are then included in the standard bulk formulae that are used to calculate the heat and freshwater fluxes into our relatively high-resolution ¼° ocean. The simulation is 120 yrs long, beginning in 1980, and so should be well spun up.

We show fields of mean kinetic energy and Montgomery function in Fig. 12a and b, as for the present-day simulations discussed earlier. The mean kinetic energy at 1650m depth is rather different in this run from the others. Flow is generally weaker, and seems be striated, even in the ocean interior. There is however a reasonably strong western boundary current.

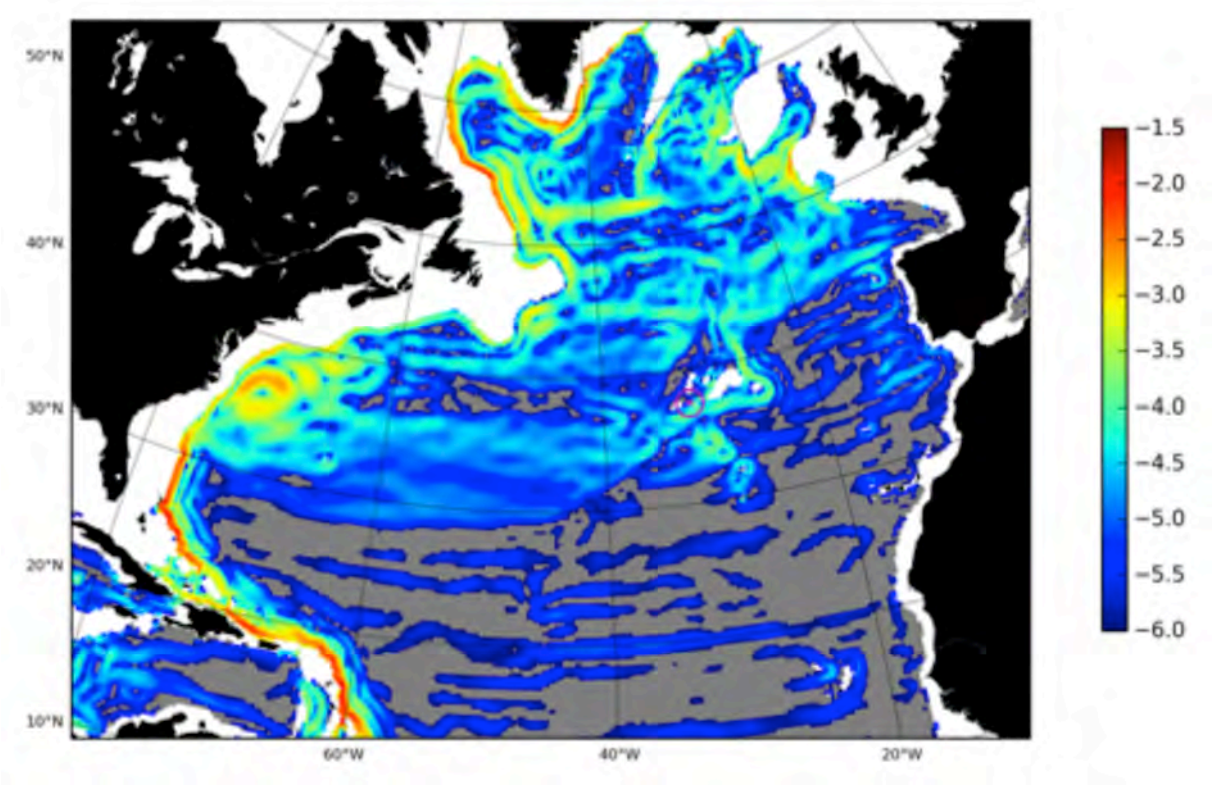

Figure 12: Log_{10} of the mean kinetic energy in m^2s^{-2}. Greyed out areas denote values less than 10^{-6} i.e speeds less than ~1.4 mm s^{-1}.

5.1 Results from the 1/4° model forced by the atmosphere of the 2090s

The 800,000 particles seeded as in the previous run were then tracked by the ARIANE trajectory program over the 10 year period 2090–2099, using 5-day velocity means from the eddy-resolving 1/4° horizontal resolution NEMO configuration. Again ~5% of the particle positions at 2, 5 and 10 years are shown in 3D in Fig. 13a, b and c.

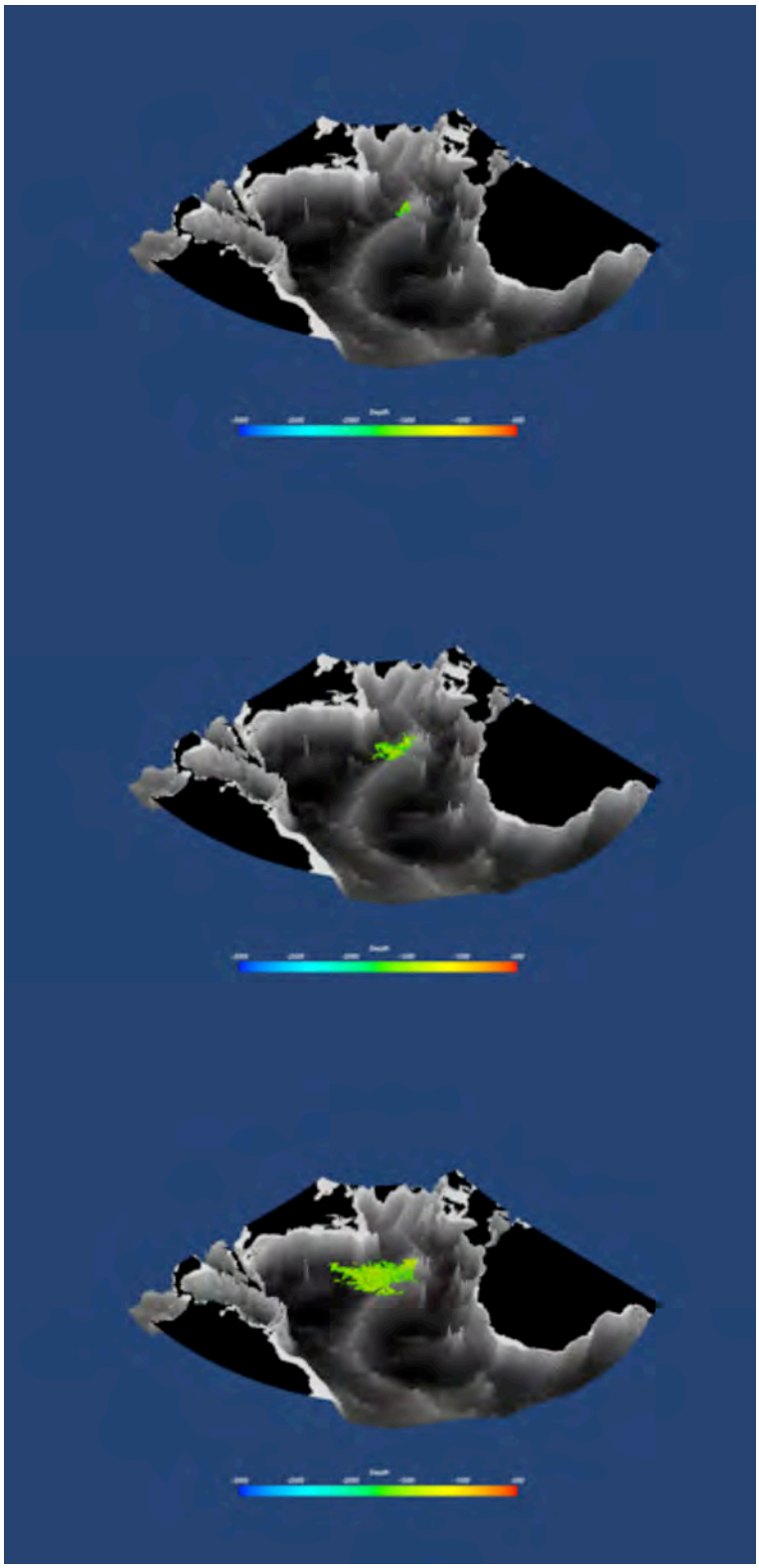

Figure 13: Particle positions at a. (top) 2 yrs, b (middle) 5 yrs and c (bottom) at 10 yrs for the ¼° model run with forcing from 2090–2099.

Dispersion of the particles is evidently much weaker in this particular run. This is consistent with the slower flows seen in Fig. 12a in comparison with Fig. 8: the mean kinetic energy is about an order of magnitude less in the interior. More detailed comparison of the two ¼° runs with present and 2090–2099 forcing is required to understand what is causing this difference, and whether it results from the different forcing or differences in other model parameters.

Vertical spreading and upwards movement similar to the other ¼° run is evident in the histogram Fig. 14a, and dispersion in density is also similar (Fig. 14b).

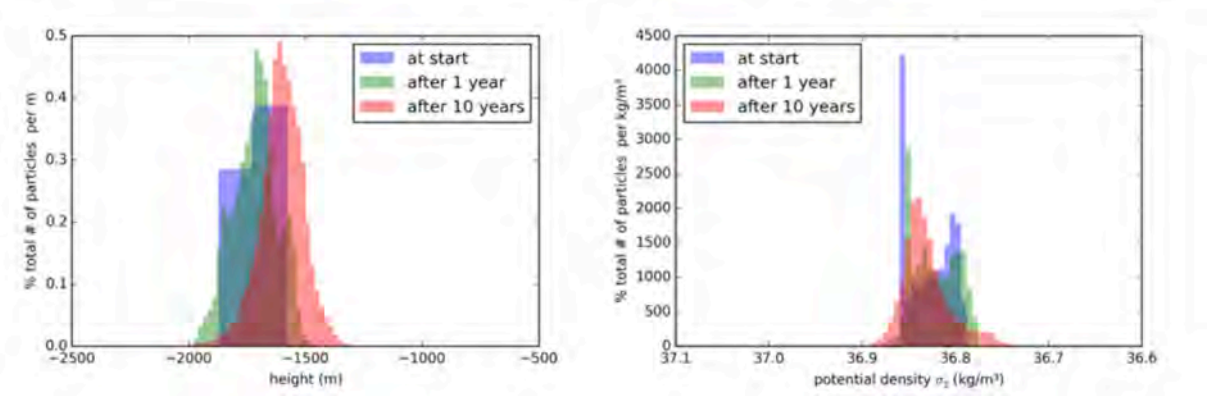

Figure 14a (left panel): Histogram of particle density against depth, and 14b (right panel) against potential density referenced to 2000 m for the ¼° projection run.

Lateral dispersion is weaker as was obvious from the particle cloud. Fig. 15a shows that particles still move westward, but much shorter distances than in the present-day ¼° model (Fig. 11). Dispersion is again far weaker than in the 1/12° model (Fig. 6). Fig. 15b emphasizes how most of the particle load remains close to the release site, with 36% in the bin SW of the release site and 24% remaining in the 10° by 10° bin encompassing the release site. It is interesting however, that it is the eddy-resolving model has the highest percentage of particles (32%) within the bin encompassing the release site.

6. Discussion and conclusions

The results of the eddy-resolving run are perhaps the clearest. They show some dispersion of the particles throughout the whole of the western North Atlantic subtropical gyre, mostly along the 36.8-36.9 σ_2 potential density surface, about 1900–1600 m deep. Despite the wide dispersion, a substantial fraction of the particles in fact remain fairly close to the release site, with 32% still within the 10° by 10° box covering this site after 10 years. All the particles described here were released between 1600 m depth, and the ocean floor, which was ~1800–2000m deep over the release site. The lateral spread of particles released at different depths in this range did vary, but not so much as to imply major differences in behaviour.

The ¼° model with present-day forcing had weaker but more coherent flows in the ocean interior generally, but happened to have stronger flow over the release area. As a consequence, although particles did not spread over as much as the ocean as at higher resolution, this model showed the greatest movement of tracer away from the release site, with the majority entering the heart of the subtropical gyre around 30° N, 60° W.

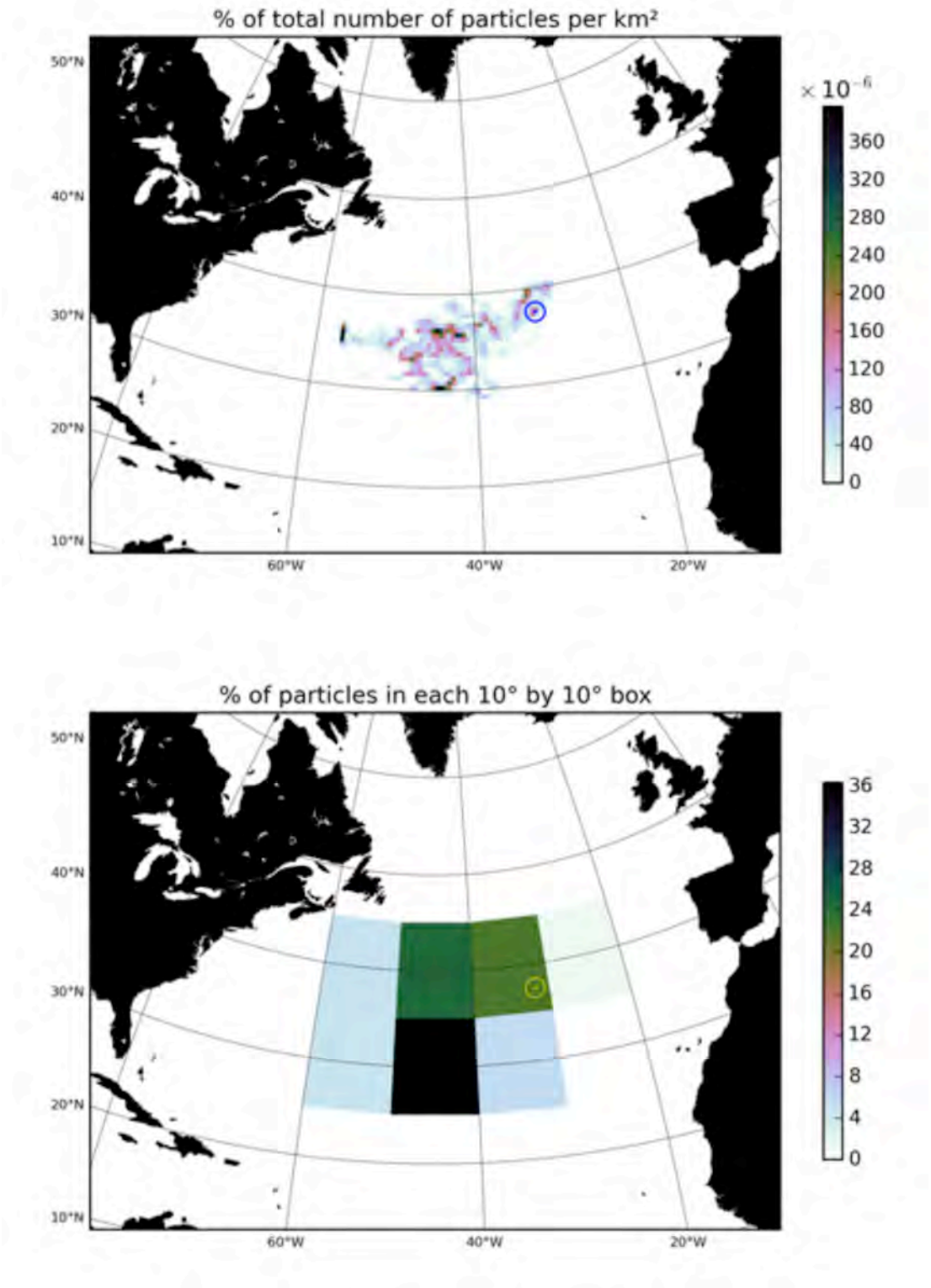

Figure 15a (top panel): Colour-shaded plot of horizontal field of vertically-integrated particle density, given as % of total number of particles per square kilometre. 15b. (bottom panel) % of particles within each of the 10° by 10° bins.

The ¼° model forced by the atmosphere of the 2090s had considerably weaker circulation and far less particle spread than the other two models, and in particular the ¼° model forced by the present-

day atmosphere. More detailed work is required to understand how much of the differences in the two models result from the different forcing and from the different model parameters.

More generally, this work emphasises the sensitivity of the results to model parameters and setup. Models do not always give as good a representation of the deep and bottom flows as we would wish, and in particular may tend to underestimate their strength (Scott et al., 2010). We intend to confront the models with the MIDAS observations to help validate and improve them.

7. Bibliography

Aksenov, Y., Ivanov, V., Nurser, G., Bacon, S., Polyakov, I., Coward, A., Naveira- Garabato, A., and Beszczynska-M¨oller, A. (2011). The Arctic Circumpolar Boundary Current. J. Geophys. Res.-Oceans, 116(C09017).

Aksenov, Y., Popova, E, A. Yool, A.J. G Nurser, T. Williams, L. Bertino and J. Bergh: Future navigability of Arctic sea routes: High-resolution projections of the Arctic Ocean and Sea Ice decline. Marine Policy, in press.

Blaker, A. T., Hirschi, J., McCarthy, G., Sinha, B., Taws, S., Marsh, R., de Cuevas, B., Alderson, S.,

Coward, A., 2015. Historical analogues of the recent extreme minima observed in the Atlantic meridional overturning circulation at 26N, Climate Dynamics, 44, 1, 457–473, doi: 10.1007/s00382-014-2274-6.

Blanke B, Raynaud S (1997) Kinematics of the Pacific Equatorial Undercurrent: a Eulerian and Lagrangian approach from GCM results. J Phys Oceanogr 27:1038–1053.

Marzocchi, A., J. J.-M. Hirschi, P. N. Holliday, S. A. Cunningham, A. T. Blaker, and A. C. Coward, 2015: The North Atlantic subpolar circulation in an eddy-resolving global ocean model. J. Mar. Syst., 142, 126-143.

McDougall, T. J.,2015. Streamfunctions for the lateral velocity vector in a compressible ocean. J. Mar. Res, 47(2):267–284.

Scott, Robert B.; Arbic, Brian K.; Chassignet, Eric P.; Coward, Andrew C.; Maltrud, Mathew; Merryfield, William J.; Srinivasan, Ashwanth; Varghese, Anson. Total kinetic energy in four global eddying ocean circulation models and over 5000 current meter records. Ocean Modelling, 32, 157–169.

A. Yool, E. E. Popova, and A. C. Coward. Future change in ocean productivity: Is the Arctic the new Atlantic? J. Geophys. Res. , in press.